Efficient N_2O_5 Uptake and NO_3 Oxidation in the Outflow of Urban Beijing

Haichao Wang[1], Keding Lu[1*], Song Guo[1], Zhijun Wu[1], Dongjie Shang[1], Zhaofeng Tan[1], Yujue Wang[1], Michael Le Breton[2], Mingjin Tang[3], Yusheng Wu[1], Jing Zheng[1], Limin Zeng[1], Mattias Hallquist[2], Min Hu[1] and Yuanhang Zhang[1,4]

[1]State Key Joint Laboratory or Environmental Simulation and Pollution Control, College of Environmental Sciences and Engineering, Peking University, Beijing, China.

[2]Department of Chemistry and Molecular Biology, University of Gothenburg, Gothenburg, Sweden

[3]State Key Laboratory of Organic Geochemistry and Guangdong Key Laboratory of Environmental Protection and Resources Utilization, Guangzhou Institute of Geochemistry, Chinese Academy of Sciences, Guangzhou, China

[4]CAS Center for Excellence in Regional Atmospheric Environment, Chinese Academy of Sciences, Xiamen, China

*_Corresponding to_: Keding Lu (k.lu@pku.edu.cn)

Abstract. Nocturnal reactive nitrogen compounds play an important role in regional air pollution. Here we present the measurements of dinitrogen pentoxide (N_2O_5) associated with nitryl chloride ($ClNO_2$) and particulate nitrate (pNO_3^-) in a suburban site of Beijing in the summer of 2016. High levels of N_2O_5 and $ClNO_2$ were observed in the outflow of the urban Beijing air masses, with 1-min average maxima of 937 pptv and 2900 pptv, respectively. The N_2O_5 uptake coefficients, γ, and $ClNO_2$ yield, f, were experimentally determined from the observed parameters. The N_2O_5 uptake coefficient ranged from 0.012 to 0.055, with an average of 0.034 ± 0.018, which is in the upper range of previous field studies reported in North America and Europe but is a moderate value in the North China Plain (NCP), which reflects efficient N_2O_5 heterogeneous processes in Beijing. The $ClNO_2$ yield exhibited high variability, with a range of 0.50 to unity and an average of 0.73 ± 0.25. The concentration of the nitrate radical (NO_3) was calculated assuming that the thermal equilibrium between NO_3 and N_2O_5 was maintained. In NO_x-rich air masses, the oxidation of nocturnal biogenic volatile organic compounds (BVOCs) was dominated by NO_3 rather than O_3. The production rate of organic nitrates (ONs) via NO_3+BVOCs was significant, with an average of 0.10 ± 0.07 ppbv h^{-1}. We highlight the importance of NO_3 oxidation of VOCs in the formation of ONs and subsequent secondary organic aerosols in summer in Beijing. The capacities of BVOCs oxidation and ONs formation are maximized and independent of NO_x under a high NO_x/BVOCs ratio condition (>10), which indicates that reduction of NO_x emissions cannot help reduce the nocturnal formation of ONs.

1. Introduction

It has been well recognized that reactive nitrogen compounds, specifically the nitrate radical (NO_3) and dinitrogen pentoxide (N_2O_5), play a key role in nighttime chemistry (Wayne et al., 1991; Brown and Stutz, 2012). NO_3 is the most important oxidant in the nighttime and can be considered the nighttime analogue of the hydroxyl radical (OH) for certain VOCs (Wayne et al., 1991; Benton et al., 2010). NO_3 can initiate the removal of many kind of anthropogenic and biogenic emissions after sunset. In the NO_x-rich plumes, NO_3 is responsible for the vast majority of the oxidation of biogenic VOCs because of its rapid reactions with unsaturated hydrocarbons (Edwards et al., 2017). NO_3 is predominantly formed by the reaction of NO_2 with O_3 (R1) and further reacts with NO_2 to produce N_2O_5 (R2). Because N_2O_5 is rapidly decomposed back into NO_2 and NO_3 (R3), NO_3 and N_2O_5 are in dynamic equilibrium in the troposphere.

$$NO_2 + O_3 \rightarrow NO_3 + O_2 \quad \text{(R1)}$$

$$NO_2 + NO_3 + M \rightarrow N_2O_5 + M \quad \text{(R2)}$$

$$N_2O_5 + M \rightarrow NO_2 + NO_3 + M \quad \text{(R3)}$$

Photolysis of NO_3 and its reaction with NO are rapid, which leads to a daytime NO_3 lifetime being shorter than 5 s with extremely low concentrations, whereas in low-NO air masses, the fate of NO_3 is mainly controlled by the mixing ratios of various VOCs and N_2O_5 heterogeneous hydrolysis because the two terms are the dominating loss pathways of NO_3 and N_2O_5. The VOCs reaction is significant downwind of an urban area or a strongly urban-influenced forested area in summer. The NO_3 oxidation of VOCs was responsible for more than 70% nocturnal NO_3 loss in Houston (Stutz et al., 2010) and contributed approximately 50% in the forest region in Germany (Geyer et al., 2001). The reactions of NO_3 with several BVOCs produce considerable amounts of organic nitrates (ONs) with efficient yields, which act as important precursors of secondary organic aerosols (SOA). The reaction of NO_3 with isoprene has a SOA mass yield of 23.8% (Ng et al., 2008). For the reaction with monoterpene, such as limonene, the SOA mass yield can reach 174% at ambient temperatures (Boyd et al., 2017). The reactions of NO_3+BVOCs are critical to the studies of aerosols on regional and global scales (Fry et al., 2009; Rollins et al., 2009; Pye et al., 2010; Ng et al., 2017). For example, ONs had extensive percentages of fine particulate nitrate (pNO_3^-) (34% - 44%) in Europe (Kiendler-Scharr et al., 2016).

The heterogeneous hydrolysis of N_2O_5 produces soluble nitrate (HNO_3 or NO_3^-) and nitryl chloride ($ClNO_2$) on chloride-containing aerosols (R4) (Finlayson-Pitts et al., 1989). This reaction is known to be an important intermediate in the NO_x removal processes (Brown et al., 2006). The pseudo-first order loss rate constant N_2O_5 via heterogeneous uptake is given in Eq. 1 (Wahner et al., 1998).

$$N_2O_5 + (H_2O \text{ or } Cl^-) \rightarrow (2 - f)\, NO_3^- + f\, ClNO_2 \quad \text{(R4)}$$

$$k_{N2O5} = 0.25 \cdot c \cdot \gamma(N_2O_5) \cdot S_a \quad \text{(Eq. 1)}$$

Where c is the mean molecule speed of N_2O_5, S_a is the aerosol surface concentration and $\gamma(N_2O_5)$ is the N_2O_5 uptake coefficient. N_2O_5 heterogeneous hydrolysis is one of the major uncertainties of the NO_3 budget since the N_2O_5 uptake coefficient can be highly variable and difficult to quantify (Brown and Stutz, 2012; Chang et al., 2011; H. C. Wang et al., 2016). Laboratory and field measurement studies have reported that the N_2O_5 uptake coefficient has large variability and ranges from <0.001 to 0.1; the

N_2O_5 uptake coefficient is subject to relative humidity (RH), particle morphology, compositions (water content, nitrate, sulfate, organic or mineral particles) and other factors (e.g., Wahner et al., 1998; Mentel et al., 1999; Hallquist et al., 2003; Thornton et al., 2003; Thornton et al., 2005; Brown et al., 2006; Bertram and Thornton, 2009; Tang et al., 2012, 2014; Gaston et al., 2014; Grzinic et al., 2015). The coupled chemical mechanisms in ambient conditions are still not well understood. $ClNO_2$ forms and accumulates with a negligible sink during the night and further photolysis and liberates the chlorine radical (Cl) and NO_2 after sunrise. Hundreds of pptv to ppbv of $ClNO_2$ can lead to several ppbv of O_3 enhancement and significant primary RO_x production (Osthoff et al., 2008; Thornton et al., 2010; McLaren et al., 2010; Riedel et al., 2014; Sarwar et al., 2014; Tham et al., 2016).

Large amounts of NO_x have been emitted for the past several decades in China, but comprehensive field studies of the nighttime chemical processes of reactive nitrogen oxides remain sparse. Previous studies have found high mixing ratios of NO_3 associated with high NO_3 reactivity in the megacities in China, including Shanghai, the Pearl River Delta (PRD) and Beijing (Li et al., 2012; Wang et al., 2013; Wang et al., 2015). N_2O_5 concentration was elevated in Beijing (H. C. Wang et al., 2017a; H. C. Wang et al., 2017c) but was moderate in other places of North China Plain (NCP), such as Wangdu, Jinan and Mount Tai (Tham et al., 2016; X. F. Wang et al., 2017; Z. Wang et al., 2017). Recently, the N_2O_5 uptake coefficients were determined to be very high, even up to 0.1 in NCP, but the reason is still not well studied (H. C. Wang et al., 2017c; X. F. Wang et al., 2017; Z. Wang et al., 2017). Reactive N_2O_5 chemistry was also reported in Hong Kong, and showed the highest field-observed N_2O_5 concentration to date (T. Wang et al., 2016; Brown et al., 2016). Observations and model simulations revealed that fast heterogeneous uptake of N_2O_5 is an important pathway of pNO_3^- formation in China (H. C. Wang et al., 2017b; H. C. Wang et al., 2017c; Z. Wang et al., 2017; Su et al., 2017); the reaction also contributed significantly to removal (Z. Wang et al., 2017; Brown et al., 2016). Moreover, chlorine activation from N_2O_5 uptake had a significant effect on daytime photolysis chemistry in China (Xue et al., 2015; Li et al., 2016; Tham et al., 2016; T. Wang et al., 2016).

In this study, to quantify the contribution of NO_3 and N_2O_5 chemistry to the atmospheric oxidation capacity and the NO_x removal process in the outflow of urban Beijing, we reported the measurement of N_2O_5, $ClNO_2$, and related species in the surface layer of a suburban site in Beijing and determined the N_2O_5 heterogeneous uptake coefficients and $ClNO_2$ yields. The nighttime NO_3 oxidation of biogenic VOCs and its impact on the ONs formation in the NO_x-rich region were diagnosed. Finally, the nighttime NO_x removal via the NO_3 and N_2O_5 chemistry was estimated and discussed.

2. Method

2.1 The site

Within the framework of a Sino-Sweden joint research project, “Photochemical Smog in China”, a summer field campaign was conducted in Beijing to enhance our understanding of the secondary chemistry via photochemical smog and the heterogeneous reactions (Hallquist et al., 2016). The data presented here were collected at a regional site, PKU-CP (Peking University Changping campus), from 23 May to 5 June 2016. The measurement site is located in the northern rural area of Beijing, approximately 45 km from the city center; the closest road is approximately 1 km to the south, and there are no major industry surroundings (Figure. 1). The site is surrounded to the north, east and west by mountains. The general feature of this site is that it captures air masses with strong influences from

both urban and biogenic emissions. Instruments were set up on the fifth floor of the main building of the campus with inlets approximately 12 m above the ground. Time is given in this paper as CNST (Chinese National Standard Time = UTC+8 h). During the campaign, sunrise was at 05:00 CNST and sunset was at 19:30 CNST.

2.2 Instrument setup

A comprehensive suite of trace gas compounds and aerosol properties was measured in the field study, and the details are listed in Table 1. N_2O_5 was measured by a newly developed cavity enhanced absorption spectrometer (CEAS; H. C. Wang et al., 2017a). In the CEAS, ambient N_2O_5 was thermally decomposed to NO_3 in a perfluoroalkoxy alkanes (PFA) tube (length: 35 cm, I.D.: 4.35 mm) heated to 120 °C and was then detected within a PFA resonator cavity; the cavity was heated to 80 °C to prevent NO_3 reacting back to N_2O_5. Ambient gas was sampled with a 1.5-m sampling line (I.D.: 4.35 mm) with a flow rate of 2.0 L min^{-1}. NO was injected for 20 seconds to destroy NO_3 from N_2O_5 thermal decomposition in a 5-minute cycle, and the corresponding measurements were then used as reference spectra. A Teflon polytetrafluoroethylene (PTFE) filter was used in the front of the sampling module to remove ambient aerosol particles. The filter was replaced with a fresh one every hour to avoid the decrease of N_2O_5 transmission efficiency due to aerosol accumulation on the filter. The limit of detection (LOD) was 2.7 pptv (1σ), and the measurement uncertainty was 19%.

$ClNO_2$ and N_2O_5 were also detected using a Time of Flight Chemical Ionization Mass Spectrometer (ToF-CIMS) with the Filter Inlet for Gas and AEROsols (FIGAERO; Lopez-Hilfiker et al., 2014; Bannan et al., 2015). Briefly, the gas phase species were measured via a 2-m-long, 6-mm-outer-diameter PFA inlet while the particles were simultaneously collected on a Teflon filter via a separate 2-m-long, 10-mm-outer-diameter copper tubing inlet; both had flow rates of 2 L min^{-1}. The gas phase was measured for 25 minutes at 1 Hz, and the FIGAERO instrument was then switched to place the filter in front of the ion molecule region; it was then heated incrementally to 200 °C to desorb all the mass from the filter to be measured in the gas phase, which resulted in high-resolution thermo grams. Formic acid calibrations were performed daily using a permeation source maintained at 40 °C. Post-campaign laboratory calibrations of N_2O_5 were first normalized to the campaign formic acid calibrations to account for any change in sensitivity (Le Breton et al., 2014). Then, $ClNO_2$ measurements were quantified by passing the N_2O_5 over a wetted NaCl bed to produce $ClNO_2$. The decrease in N_2O_5 from the reaction with NaCl was assumed to be equal to the concentration of $ClNO_2$ produced (i.e., 100% yield). The sensitivities of the CIMS to N_2O_5 and $ClNO_2$ were found to be 9.5 and 1.2 ion counts per pptv Hz^{-1}, respectively, with errors of 23% and 25% for $ClNO_2$ and N_2O_5, respectively. The LOD for $ClNO_2$ and N_2O_5 were 16 and 8 pptv, respectively. An intercomparison of N_2O_5 measurements between the CEAS and FIGAERO-ToF-CIMS showed good agreement; a companion paper on chlorine photochemical activation during this campaign gives detailed intercomparison results of N_2O_5 measured by the two different techniques (Le Breton et al., 2018).

Sub-micron aerosol composition ($PM_{1.0}$), including nitrate, sulfate, chloride, ammonium and organic compounds, were measured by a High Resolution Time of Flight Aerosol Mass Spectrometer (HR-ToF-AMS) (De Carlo et al, 2006, Zheng et al., 2017). Particle number and size distribution (PNSD) was measured by a scanning mobility particle sizer (SMPS, TSI 3936) and an aerosol particle sizer (APS, TSI 3321) (Yue et al., 2009). SMPS measured the particles in the range between 3.5 nm

and 523.3 nm in diameter, and APS measured the particles with a diameter range from 597.6 nm to 10.0 μm. S_a was calculated based on the dry-state particle number and geometric diameter in each size bin (3.5 nm - 2.5 μm). Dry-state S_a was corrected to wet particle-state S_a for particle hygroscopicity by a growth factor. The growth factor, $f(RH)=1 + 8.77 \times (RH/100)^{9.74}$, was derived from the measurement of aerosol extinction as a function of RH in autumn in Beijing and is valid for 30% < RH < 90% (Liu et al., 2013). The uncertainty of the wet aerosol surface areas was estimated to be ~30%, associated from the error from dry PNSD measurement (~20%) and the growth factor (~20%). During this measurement, fine particles below 500 nm contributed to more than 90% of the total S_a.

VOCs were measured by Proton Transfer Reaction Mass Spectrometry (PTR-MS) with a time resolution of 5 minutes (de Gouw and Warneke et al., 2007; Wang et al., 2014). A commercial instrument (Thermo Electron model 42i) equipped with a molybdenum-catalytic converter was used to monitor NO_x. The LODs were 60 pptv (1 min) for NO and 300 pptv (1 min) for NO_2, with both at a 20% precision (Tan et al., 2017). The molybdenum-catalytic technique not only converts NO_2 to NO but also converts ambient NO_y such as peroxyacetyl nitrate (PAN) and HNO_3. Therefore, the measured NO_2 concentration corresponded to $NO_2 + NO_y$ and was normally higher than the real concentration, especially in an aged air mass with high NO_x conditions. In this study, we used a factor of 0.6 to correct the nighttime NO_2 concentration (a detailed explanation is in the Support Information Text S1 and Figure S1). The correction factor (0.6) used to be the averaged scaled value of the correction factors during nighttime, the standard deviation of the daytime correction factor for all the air masses experienced at Changping site was determined to be 0.27 (1σ), which extended to nighttime and result in an uncertainty of correction to be 45%. The uncertainty of NO_2 is therefore about 50% when further included the associated measurement uncertainty from calibrations. O_3 was measured by a commercial instrument using ultraviolet (UV) absorption (Thermo Electron model 49i); the LOD was 0.5 ppbv, with an uncertainty of 5%. The mass concentration of $PM_{2.5}$ was measured using a standard Tapered Element Oscillating Microbalance (TEOM, 1400A analyzer). Meteorological parameters included relative humidity, temperature, pressure, wind speed, and wind direction and were available during the campaign. Photolysis frequencies were calculated from the spectral actinic photon flux density measured by a spectroradiometer (Bohn et al., 2008).

3. Results

3.1 Overview

During the campaign, the meteorological conditions of the site was high temperature and low relative humidity (RH); the temperature ranged from 10 - 34 °C and was 23 ± 5 °C on average, and RH ranged from 10% - 80%, with an average of 37% ± 15%. Because of the special terrain of the observation site, the local wind was measured by the in situ meteorological stations; the site has a typical mountain-valley breeze that cannot reflect the general air mass movement patterns at slightly higher altitudes. Figure S2 shows the calculated backward trajectories using the Hybrid Single-Particle Lagrangian Integrated Trajectory (HYSPLIT) model (Draxler and Rolph, 2003); these images show the 24-h backward particle dispersion trajectories for 12:00 local time (CNST) as the starting time during May 23 - July 5, 2016. According to the results of HYSPLIT, the arrivals of air masses were mainly from the northwest and the south. Therefore, we meteorologically separated the measurement period into

two parts. The first three days show that the air masses came from the north or northwest; the air masses represent the background region (defined as Background Air Mass, BAM). The air masses after May 26 originated from the polluted NCP and passed over urban Beijing; they were characterized by large NO_x emissions and severe photochemical pollution (defined as Urban Air Mass, UAM).

The time series of N_2O_5, $ClNO_2$ and other relevant species are shown in Figure 2, and nighttime statistical results are listed in Table S1. The daily 8-h maximum of O_3 concentration exceeded 93 ppbv (Chinese national air quality standard) for 8 of 12 days, and all the O_3-polluted air masses came from the urban region. When the air masses were from the background region, the daily maximum of O_3 was only approximately 60 ppbv, much lower than that from the urban region. The NO_2 concentration was elevated, with a nocturnal average value over 10 ppbv during the urban air mass period. The nocturnal nitrate radical production rate, $P(NO_3)$, was large, with an average of 1.2 ± 0.9 ppbv h^{-1}, which is comparable with rates previously reported in the NCP and Hong Kong (Tham et al., 2016; Brown et al., 2016; Z. Wang et al., 2017; X. F. Wang et al., 2017). The daily peaks of N_2O_5 were 100-500 pptv most nights; the maximum of 937 pptv in a 1-min average was observed near 20:00 on the early night of June 2, when the $P(NO_3)$ was up to 4 ppbv h^{-1}. The average mixing ratio of N_2O_5 was 73 ± 90 pptv, which is much higher than recent measurements reported in North China (Tham et al., 2016; X. F Wang et al., 2017; Z. Wang et al., 2017) but much lower than that observed in the residual layer of the outflow from the PRD region, where the N_2O_5 was up to 7.7 ppbv (T. Wang et al., 2016). With an elevated O_3 mixing ratio in the first half of the night, the NO lifetime was only several minutes, and the mixing ratio of NO concentration was observed below the detection limit. During the second half of the night when the O_3 concentration was consumed to low concentration, high levels of NO could occasionally be observed, and N_2O_5 dropped to zero because of the fast titration by NO, such as the events that occurred on the second half of the nights of May 24, 28, 30. The $PM_{2.5}$ mass concentration was moderate during the measurement period, with an average of 26 ± 21 μg m^{-3}, and the average aerosol surface area was 560 ± 340 μm^2 cm^{-3}. Elevated $ClNO_2$ was observed to have a daily maximum 1-min average of over 800 pptv during the urban air masses period; the campaign maximum of up to 2900 pptv was observed on the morning (05:30) of May 31, which implied that fast N_2O_5 heterogeneous hydrolysis and effective $ClNO_2$ yields are common in Beijing. The level of $ClNO_2$ was comparable with the results in NCP (Tham et al., 2016; X. Wang et al., 2017; Z. Wang et al., 2017) but slightly higher than that measured in coastal (e.g., Osthoff et al., 2008) and inland sites (e.g., Thornton et al., 2010) in other regions of the world.

3. 2 Mean diurnal profiles

The mean diurnal profiles of the measured NO_2, O_3, N_2O_5, $ClNO_2$ and the particle chloride content are shown in Figure 3, as well as the calculated NO_3 based on the thermal equilibrium of NO_2, NO_3 and N_2O_5. The left panel show the average results of the BAM period, and the right panels show those of the UAM period. The NO_2 and O_3 from the UAM were much higher than were those from the BAM, as were the mixing ratios of N_2O_5, NO_3 and $ClNO_2$. The daily variation tendencies of those species in the two kinds of air masses were similar. N_2O_5 began to accumulate in the late afternoon and increased sharply after sunset. A peak occurred near 20:00 and decreased below the instrument detection limit at sunrise; the N_2O_5 maxima occurred at a similar time to our previous observation in urban Beijing (H. C. Wang et al., 2017c); however, the N_2O_5 decrease rate after the peak time was much slower than that

in urban Beijing, where the N_2O_5 dropped to almost zero in 2-4 hours, which suggests a relatively slow N_2O_5 loss rate in suburban Beijing. The daily average peaks of N_2O_5 during the BAM period and the UAM period were approximately 75 pptv and 150 pptv, respectively. The calculated NO_3 diurnal profile was quite similar to that of N_2O_5, and the daily average peaks of NO_3 during the BAM and UAM periods were approximately 11 pptv and 27 pptv, respectively. The uncertainty of NO_3 calculation was estimated to be 67% according to Eq. 2 which is dominated by uncertainty of the NO_2 concentrations

$$\frac{\Delta[NO_3]}{[NO_3]} = \sqrt{\left(\frac{\Delta[N_2O_5]}{[N_2O_5]}\right)^2+\left(\frac{\Delta[NO_2]}{[NO_2]}\right)^2 + \left(\frac{\Delta[O_3]}{[O_3]}\right)^2 + \left(\frac{\Delta K_{eq}}{K_{eq}}\right)^2} \quad \text{(Eq. 2)}$$

The observed $ClNO_2$ concentrations showed a clear increase after sunset and reached a maximum before sunrise for BAM period while reached a maximum around midnight for the UAM period. The diurnal peak of $ClNO_2$ in the BAM period was approximately 125 pptv, whereas the diurnal peak of $ClNO_2$ was over 780 pptv in the UAM period and approximately 6 times as high as that in the UAM period. Particle chloride (Cl^-) is regarded as a key factor that affected the $ClNO_2$ yield on aerosol surface. Higher particle chloride led to higher $ClNO_2$ yield and promoted the N_2O_5 conversion to $ClNO_2$ (e.g., Finlayson-Pitts et al., 1989; Behnke et al., 1997), whereas the particle chloride content during the measurement was below 60 pptv and was much lower than the mixing ratio of $ClNO_2$. The HYSPLIT model results showed that the air masses had almost always continental conditions; as was mentioned above, fine particles dominated the S_a, which meant that large amounts of the particle chloride were not replenished by NaCl from marine sources but possibly by gas-phase HCl (Ye et al., 2016). Cl^- was found to be correlated strongly with CO and SO_2, likely to originate from an anthropogenic source, such as power plants or combustion sources (Le Breton et al., 2018). The required nocturnal source of Cl^- to support the $ClNO_2$ production is further estimated through its loss rate. The $\gamma \times f$ was set to the campaign average value (0.019) (see Sect. 4.1), and real-time Cl^- loss rate via N_2O_5 can be calculated based on the measured N_2O_5 and S_a by Eq.3.

$$L[Cl^-] = (\gamma \times f) \cdot \int_{t_{sunset}}^{t_{sunrise}} \frac{C \cdot S_a}{4} [N_2O_5]\,dt \quad \text{(Eq. 3)}$$

Here the $L(Cl^-)$ denotes the integral Cl^- loss to form the $ClNO_2$ per night. The required source term of the Cl^- need to support the $ClNO_2$ formation during the campaign was range from (0.5 - 4.0 ppbv per night) with (1.7 ± 2.3 ppbv per night) on average. The gas phase HCl predicted by the ISORROPIA II model showed that the HCl concentration near sunset period was high enough (much larger than 2 ppbv) to support the $ClNO_2$ formation (Figure. S3). Note that up to 10 ppbv of HCl was observed in the urban Beijing in September, 2016, we believe that the potential particle Cl^- source was sufficient and gas-phase HCl was possibly the main particle chloride source by the acid displacement reaction. After sunrise, $ClNO_2$ was photolyzed and decreased with the increasing photolysis intensity; However, the $ClNO_2$ can still survive until noon with the averaged daily maximum of $J(ClNO_2)$ to be 1.7×10^{-4} s^-

[1]. Similar to the studies reported in London, Texas and Wangdu (Bannan et al., 2015; Faxon et al., 2015; Tham et al., 2016), we observed sustained elevated $ClNO_2$ events after sunrise in 5 of 12 days. For example, on the morning of May 30, $ClNO_2$ increased after sunrise and peaked at approximately 8:00 am, with a concentration over 500 pptv, which was impossible from the local chemical formation since N_2O_5 dropped to almost zero and the needed N_2O_5 uptake coefficients were unrealistically high. Previous work has suggested that abundant $ClNO_2$ produced in the residual layer at night and downward transportation in the morning may help to explain this phenomenon (Tham et al., 2016).

3.3 Variation of N_2O_5 in the background air masses

During the BAM period, the O_3 concentration was well in excess of NO_2. In the NO_3 and N_2O_5 formation processes, the limited NO_2 in high O_3 region indicates that the variation of NO_2 is more essential to the variation of the N_2O_5 concentration. As shown in Figure 4, during the night of May 24 (20:00 - 04:00), the local emission of NO was negligible. O_3 concentration was larger than 25 ppbv, much higher than NO_2 and free of the local NO emission. The N_2O_5 concentration was highly correlated with NO_2 (R^2 = 0.81) and the NO_3 production rate (R^2 = 0.60), suggests the N_2O_5 concentration was solely response to the NO_2 concentration in the background air mass when enough O_3 is presented.

3.4 Elevated $ClNO_2$ to N_2O_5 ratio

Large day-to-day variabilities of N_2O_5 and $ClNO_2$ were observed during the measurement period. Following the work of Osthoff et al. (2008), Mielke et al. (2013), Phillips et al. (2012) and Bannan et al. (2015), we used the concentration ratio of $ClNO_2$ to N_2O_5, to describe the conversion capacity of N_2O_5 to $ClNO_2$. The nighttime peak values and mean values of $ClNO_2$: N_2O_5 were used to calculate the ratios are listed in Table S2, the calculation period is from 19:30 to the next day 05:00. The average nighttime ratio ranged from 0.7 to 42.0, with a mean of 7.7 and a median of 6.0. The $ClNO_2$ formation was effective, with $ClNO_2$:N_2O_5 ratios larger than 1:1 throughout the campaign, except for the night of May 26, when the ratio was 0.7:1. Previous observations of the $ClNO_2$:N_2O_5 ratios are summarized in Table 2. Compared with the results conducted in similar continental regions in Europe and America (0.2 - 3.0), the ratios in this work were significantly higher and consistent with the recent studies in the NCP (Tham et al., 2016; X. F. Wang et al., 2017; Z. Wang et al., 2017), which suggests that high $ClNO_2$: N_2O_5 ratios were ubiquitous in the NCP and implies that the $ClNO_2$ yield via N_2O_5 uptake is efficient.

4. Discussion

4.1 Determination of N_2O_5 uptake coefficients

A composite term, $\gamma \times f$, was used to evaluate the production of $ClNO_2$ from N_2O_5 heterogeneous hydrolysis (Mielke et al., 2013). $\gamma \times f$ was estimated by fitting the observed $ClNO_2$ in a time period when the nighttime concentrations of $ClNO_2$ kept increasing. The increased $ClNO_2$ was assumed to be solely from the N_2O_5 uptake. The fitting was optimized by changing the input of $\gamma \times f$ associated with

the measured N_2O_5 and S_a, until the $ClNO_2$ increasing was well reproduced (Eq. 4). Here t_0 and t denote the start time and end time, respectively, $[ClNO_2](t_0)$ is the observed concentration at t_0 and set as the fitting offset. The calculation time duration was normally several hours, and the derived $\gamma \times f$ was found to be constant with small uncertainties for optimization (see Table S3). It is worth to be noticed that both the N_2O_5 and S_a is not necessary to be stable in this calculation due to the use of integration.

$$[ClNO_2](t) = [ClNO_2](t_0) + (\gamma \times f) \cdot \int_{t_0}^{t} \frac{C \cdot S_a}{4} [N_2O_5]\,dt \qquad \text{(Eq. 4)}$$

The values of $\gamma \times f$ had moderate variability, a range from 0.008 - 0.035 and an average of 0.019 ± 0.009. Table 3 summarizes the $\gamma \times f$ values derived in the previous field observations. The value in suburban Germany was between 0.001 and 0.09, with the average of 0.014 (Phillips et al., 2016), and the average value in Mt. Tai, China, was approximately 0.016 (Z. Wang et al., 2017). Therefore, the average value in this study was comparable with that of the two suburban sites, whereas in an urban site of Jinan, China (X. F. Wang et al., 2017), the value was lower than 0.008 and comparable with that in the CalNex-LA campaign. The three sets of $\gamma \times f$ values from suburban regions were approximately twice as large as those in urban regions, which implies that the $ClNO_2$ formation efficiency in the aged air masses in suburban regions were more efficient than in the urban region. The difference of the overall yield between the two regions may have been caused by (1) the particle morphology variation because of particle aging, such as the particle mixing state, O: C ratio, particle viscosity and solubility (Riemer et al., 2009; Gaston et al., 2014; Grzinic et al., 2015) or (2) the particle compound variation such as the liquid water content and the Cl^- content. The liquid water content and the Cl^- content were proposed to affect the $ClNO_2$ yield because those particle physicochemical properties were reported to affect the N_2O_5 uptake coefficient (Bertram and Thornton, 2009).

According to reaction R4, pNO_3^- and $ClNO_2$ were formed by N_2O_5 heterogeneous uptake, with yields of 2 - f and f, respectively. Following the recent work of Phillips et al., (2016), we used the observed pNO_3^- and $ClNO_2$ formation rates to derive individual γ and f. The calculations assumed that the relevant properties of the air mass are conserved and that the losses of produced species are negligible; additionally, the N_2O_5 uptake coefficients and the $ClNO_2$ yield are independent of particle size. The nights characterized by the following two features were chosen for further analysis: (1) for some nights, significant correlations between pNO_3^- and $ClNO_2$ were presented ($R^2 > 0.5$); while on the other nights, the R^2 were always smaller than 0.2, which is not meet the theoretical hypothesis of this method. In this case, we chose the nights with high correlations. (2) An equivalent or increase in ammonium was accompanied by an increase of pNO_3^-, which suggested that the gas-phase ammonia was repartitioned to form ammonium nitrate and suppress the release of HNO_3. The rich-ammonia conditions in Beijing (Liu et al., 2017) demonstrated that the degassing of HNO_3 at night can be effectively buffered by the high concentrations of ammonia presented in the NCP. For the nocturnal HNO_3 uptake effect, the daytime produced HNO_3 will be soon in a new equilibrium with the particulate nitrate within a time scale of about hundred seconds; the nighttime source of HNO_3 are normally negligible except there are significant unknown OH sources at night. Both the gas-particle repartitioning of HNO_3 and nighttime produced HNO_3 will result in the overestimation of γ and underestimation of f. During this campaign, five nights were eligible for the following analysis. Based on the observational data of N_2O_5, $ClNO_2$, pNO_3^- and S_a with the time resolution of 5 minutes, the

formations of pNO_3^- and $ClNO_2$ were calculated and integrated to reproduce the increasing of pNO_3^- and $ClNO_2$ with estimated values for γ and f. The offset of particle nitrate and $ClNO_2$ is the measured particle nitrate and $ClNO_2$ concentration at the start time. The γ and f were optimized based on the Levenberg-Marquardt algorithm until good agreement between the observed and predicted concentrations of pNO_3^- and $ClNO_2$ was obtained (Phillips et al., 2016). Figure 5 depicts an example of the fitting results on May 28, the predicted N_2O_5 uptake coefficient and $ClNO_2$ yield were 0.017 and 1.0, respectively. The uncertainty on each individual fitting is varied from 55% - 100% due to the variability and measurements uncertainties of pNO_3^- and $ClNO_2$. Five sets of values of γ and f obtained are listed in Table 4. N_2O_5 uptake coefficients ranged from 0.012 - 0.055, with an average of 0.034 ± 0.018, and the $ClNO_2$ yield ranged from 0.50 to unity, with an average of 0.73 ± 0.25. The errors from each derivation were about approximately 55% and came from the field measurements of S_a, N_2O_5, pNO_3^- and $ClNO_2$.

The average γ value was consistent with the results derived by the same method in a rural site in Germany (Phillips et al., 2016) but was higher than that found in previous studies in the UK and North America that used different derivation methods; these methods included the steady state lifetime method (Morgan et al., 2015; Brown et al., 2006, 2009), the iterated box model (Wagner et al., 2013) and direct measurement based on an aerosol flow reactor (Bertram et al., 2009; Riedel et al., 2012). The steady state lifetime method is very sensitive to NO_2 concentration, and since the NO_2 measurement suffered with ambient NOy interference, we did not apply the steady state lifetime method in this study (Brown et al., 2003). Nonetheless, the derived γ in Beijing showed good agreement with the recent results derived by the steady state method in Jinan and Mt. Tai (X. F. Wang et al., 2017; Z. Wang et al., 2017). The consistency eliminates the discrepancy possibly brought by the differences of analysis methods. Therefore, we suggest that fast N_2O_5 uptake was a ubiquitous feature that existed in the NCP. In this study, sulfate is the dominant component of $PM_{1.0}$, accounting for more than 30% of its mass concentration, which may be the reason of elevated N_2O_5 uptake coefficient presented in Beijing, like the result in high sulfate air mass over Ohio and western Pennsylvania (Brown et al., 2006). Previous studies have shown that the N_2O_5 uptake coefficient strongly depends on the liquid water content, the pNO_3^- and organic mass. Liquid water content promotes N_2O_5 uptake, whereas pNO_3^- and organic mass inhibit N_2O_5 uptake (e.g., Thornton et al., 2003, Wahner et al., 1998; Bertram and Thornton, 2009). Because of the limited data set of N_2O_5 uptake coefficients in this campaign, the trends of the determined N_2O_5 uptake coefficients with the parameters mentioned above were not convincing, and more valid data is needed for further studies of the N_2O_5 uptake mechanism. With respect to f, the values are comparable with that observed in Germany (Phillips et al., 2016) and are similar with that estimated in the power plant plume in Mt. Tai with high chloride content (Z. Wang et al., 2017).

4.2 N_2O_5 lifetime and reactivity

The lifetime of N_2O_5 was estimated by the steady state method, assuming that the production and loss of N_2O_5 was in balance after a period following sunset. Eq. 5 for the steady state approximation has been frequently applied in analyzing the fate of N_2O_5 (Platt et al., 1980; Allan et al., 1999; Brown et al., 2003).

$$\tau_{ss}(N_2O_5) = \frac{1}{L_{ss}(N_2O_5)} = \frac{[N_2O_5]}{k_{NO2+O3}[NO_2][O_3]} \quad \text{(Eq. 5)}$$

Here $\tau_{ss}(N_2O_5)$ denotes the steady state lifetime of N_2O_5 and $L_{ss}(N_2O_5)$ denotes the loss term of N_2O_5 corresponding to the steady state lifetime. A numerical model was used to check the validity of the steady state approximation (Brown et al., 2003); details are given in Figure S4. The results show that the steady state can generally be achieved within 30 minutes. In this study, the steady state lifetime was only calculated from 20:00 to the next day 04:00. The time periods with NO concentration larger than 0.06 ppbv (instrument LOD) were excluded because the steady state is easily disturbed. The overall N_2O_5 loss rate ($k(N_2O_5)$) can be calculated by accumulating each individual loss term in Eq. 6, including the N_2O_5 heterogeneous hydrolysis and the reaction of NO_3 with VOCs.

$$k(N_2O_5) = \frac{\sum k_{NO3+VOCs_i}\cdot[VOCs_i]}{k_{eq}\cdot[NO_2]} + \frac{c\cdot S_a\cdot\gamma}{4} \quad \text{(Eq. 6)}$$

The NO_3 heterogeneous uptake and the loss of N_2O_5 via gas-phase reactions were assumed to be negligible (Brown and Stutz, 2012). $k_{NO3+VOCs_i}$ denotes the reaction rate constants of the reaction of NO_3+$VOCs_i$. Isoprene and monoterpene were used in this calculation.

The N_2O_5 loss rate coefficient by heterogeneous hydrolysis was calculated by using an average γ of 0.034. The time series of the steady state lifetime of N_2O_5 is shown in Figure S5. The N_2O_5 steady state lifetime ranged from <5 s to 1260 s, with an average of 270 ± 240 s, and large variability was shown during the campaign. The N_2O_5 lifetimes during the BAM period were higher than those during the UAM period, which is predictable since the clean air mass has lower N_2O_5 reactivity because of much lower aerosol loading. Two extremely short N_2O_5 lifetime cases were captured on the nights of May 30 and June 3, with peak values below 200 s throughout those nights. Figure 6 shows that the N_2O_5 lifetime had a very clear negative dependence of the ambient aerosol surface area when larger than 300 $\mu m^2\ cm^{-3}$, which indicates that the N_2O_5 heterogeneous uptake plays an important role in the regulation of N_2O_5 lifetime. The study conducted in the residual layer of Hong Kong showed a similar tendency despite the overall N_2O_5 lifetime being shorter at this site (Brown et al., 2016). Additionally, a negative dependence of N_2O_5 lifetime on RH was reported in Hong Kong but was not observed in this study (Figure S6).

Figure 7 shows the time series of the overall N_2O_5 loss rate constant as well as the N_2O_5 steady state loss rate constant. The overall N_2O_5 loss rate constant was calculated from the individual terms (Eq.3). The uncertainties of the N_2O_5 steady state loss rate constant and the overall $k(N_2O_5)$ are estimated to be 67% and 95%, respectively (Eq. 7 and Eq. 8). The largest error sources were from the corrected NO_2 measurements so that it is really important to have accurate NO_2 measurement instrument involved in the future campaigns.

$$\frac{\Delta Lss(N_2O_5)}{Lss(N_2O_5)} = \sqrt{(\frac{\Delta[N_2O_5]}{[N_2O_5]})^2 + (\frac{\Delta[NO_2]}{[NO_2]})^2 + (\frac{\Delta[O_3]}{[O_3]})^2 + (\frac{\Delta K_{eq}}{K_{eq}})^2} \quad \text{(Eq. 7)}$$

$$\frac{\Delta k(N_2O_5)}{k(N_2O_5)} = \sqrt{(\frac{\Delta[N_2O_5]}{[N_2O_5]})^2 + (\frac{\Delta[S_a]}{[S_a]})^2 + (\frac{\Delta[\gamma]}{[\gamma]})^2 + (\frac{\Delta[NO_2]}{[NO_2]})^2 + (\frac{\Delta[O_3]}{[O_3]})^2 + (\frac{\Delta[VOC_s]}{[VOC_s]})^2 + (\frac{\Delta K_{eq}}{K_{eq}})^2} \quad \text{(Eq. 8)}$$

On the night of 29 May, the steady state loss rate constant was much lower than the overall k(N_2O_5); on the nights of 28, May and 3 June, the L_{ss}(N_2O_5) calculated by the steady state method were much higher than the overall k(N_2O_5), but these discrepancies were in the range of the uncertainties. Except the case happened on the night of 30 May, when the steady state loss rate constant was about ten times higher than the overall loss rate constant, and the reason was not well understood according to the available parameters that we have detected. In general, the overall N_2O_5 loss rate constant and the steady state N_2O_5 loss rate constant were comparable taking into considerations of the uncertainties. The average N_2O_5 loss rate constant contributed by the N_2O_5 heterogeneous hydrolysis was 8.1×10^{-4} s^{-1}. The average NO_3 loss rate constant by the reaction of NO_3 with VOCs was 0.015 ± 0.007 s^{-1}, which is comparable with the previous results in suburban Beijing in 2006 (H. C. Wang et al., 2017c), in which the contribution to the N_2O_5 reactivity was 1.63×10^{-3} s^{-1}. Compared with N_2O_5 loss via direct heterogeneous hydrolysis, the indirect loss via NO_3+VOCs was dominant, accounting for approximately 67%. Because only a subset of the suite of organic species at the site was measured, the calculated loss rate constant via NO_3+VOCs represents a lower limit. Therefore, the N_2O_5 loss via NO_3+VOCs may occupy a larger proportion. The overall loss rate constant from NO_3+VOCs and N_2O_5 uptake was 2.44×10^{-3} s^{-1}, which was reasonably lower than the steady state N_2O_5 loss rate constant of 3.61×10^{-3} s^{-1}; the gap may be explained by the unmeasured reactive VOCs or the unaccounted NO that was near the instrumental limit of detection.

4.3 NO_3-induced nocturnal oxidation of VOCs

Recent studies have suggested that the fate of BVOCs after sunset is dominated by NO_x or O_3, with variation of the ratio of NO_x to BVOCs and that the nighttime oxidation is located in the transition region between NO_x-domination and O_3-domination in the United States (Edwards et al., 2017). During this campaign, the nocturnal average concentrations of isoprene and monoterpene were 156 ± 88 pptv and 86 ± 42 pptv, respectively. We used isoprene and monoterpene to represent a lower limit mixing ratio of total BVOCs; the average ratio of NO_x/BVOCs was larger than 10 and exhibited small variation during the BAM and UAM periods. The value was much higher than the critical value (NO_x /BVOC = 0.5) of the transition regime proposed by Edwards et al. (2017), which suggests that the oxidation of BVOCs in Beijing was NO_x-dominated and the nighttime fate of BVOCs was controlled by NO_3. Since the ONs formation via BVOC oxidation was mainly attributed to the NO_3 oxidation with high yield, we suggest that the ONs production capacity was maximized in the high NO_x/BVOCs region.

The pseudo first order loss rate of VOCs initialed by oxidants, k($VOCs_i$), is defined as VOCs reactivity and expressed as Eq. 9. Here, we only consider the reaction of VOCs with O_3 and NO_3. $k_{O_3+VOCs_i}$ denotes the reaction rate constants of $VOCs_i$ with O_3.

$$k(VOCs_i) = k_{NO_3+VOCs_i} \cdot [NO_3] + k_{O_3+VOCs_i} \cdot [O_3] \qquad \text{(Eq. 9)}$$

During this campaign, VOCs reactivity could be determined with the measured O_3 and calculated NO_3. Figure 8 depicts four kinds of VOCs reactivity distribution during nighttime, including the isoprene (ISO), monoterpene (MNT), the double bond at the end or terminal position of the molecule (OLT) and alkenes with the double bond elsewhere in the molecule (OLI). The reaction rates were cited from

the regional atmospheric chemistry mechanism version 2 (RACM2, Goliff et al., (2013)). Previous measurement indicated the main detectable monoterpenes were α-pinene and β-pinene in summer Beijing (personal communication with Ying Liu). Here we assumed α-pinene and β-pinene occupies half and half in the monoterpene. The average value of the rate coefficient of α-pinene and β-pinene with NO_3 was used as the rate coefficient of monoterpene with NO_3 (Atkinson and Arey, 2003). The uncertainty of the monoterpene + NO_3 rate coefficient in these air masses is thus estimated to be 50%. The uncertainty of calculated NO_3 is 67%. The uncertainty of the reaction rate efficiency of NO_3+monoterpene (50%) was calculated by the Gaussian propagation method and the overall uncertainty of monoterpene reactivity was calculated to be 85%, the uncertainties of other VOCs was calculated to be 75% by assuming the uncertainties of rate efficiencies were 30%. The VOCs reactivity were dominated by NO_3 oxidation and contributed up to 90% in total; less than 10% VOCs were oxidized by O_3 during the nighttime. Even the NO_3 concentration in the lower range, NO_3 still responsible for more than 70% nocturnal BVOCs oxidation, the results further confirmed that the oxidation of BVOCs is controlled by NO_3 rather than O_3 in summer Beijing.

For calculating nocturnal ONs production from NO_3 oxidation of isoprene and monoterpene, as well as inorganic nitrate production via N_2O_5 heterogeneous uptake over the same period, the $ClNO_2$ yield was set to the determined average value of 0.55. The organic nitrate yield of the reaction of NO_3 with isoprene was set to 0.7, from Rollins et al. (2009). The yield from the reaction of NO_3 with monoterpene was represented by NO_3 +α-pinene and was set to 0.15, following Spittler et al. (2006). Although the yield from the NO_3 oxidation of isoprene is much higher than that of monoterpene, the total ONs production was dominated by the oxidation of NO_3 with monoterpene because the reaction of NO_3 with monoterpene is much faster than that with isoprene. Because of the lack of measurement of alkenes and other VOCs that can react with NO_3 and form ONs, the calculated nighttime ONs production rate analyzed here served as lower limit estimations. Figure 9 depicts the mean diurnal profiles of the nocturnal formation rates of inorganic nitrates and ONs. The average production rate of ONs was up to 0.10 ± 0.07 ppbv h^{-1}, which was higher than that predicted in a suburban site in Beijing in 2006, with an average value of 0.06 ppbv h^{-1} (H.C. Wang et al., 2017b). In the high NO_x/BVOCs air masses, the inorganic nitrate formation was proposed to increase with the increase of sunset NO_x/BVOCs (Edwards et al., 2017). The formation rate of inorganic nitrate via N_2O_5 uptake was significant, with an average of 0.43 ± 0.12 ppbv h^{-1}, and was much larger than the organic nitrate formation. NO_x was mainly removed as the inorganic nitrate format by nocturnal NO_3-N_2O_5 chemistry in Beijing. Overall, the NO_3-N_2O_5 chemistry led to significant NO_x removal, with 0.54 ppbv h^{-1} accounted for by the organic and inorganic nitrates, and the integral NO_x removal was approximately 5 ppbv per night. Since ONs are important precursors of the secondary organic aerosols (SOA), the NO_3 oxidation was very important from the perspective of organic aerosol formation and regional particulate matter (e.g., Ng et al., 2008).

5. Conclusion

We reported an intensive field study of NO_3-N_2O_5 chemistry at a downwind suburban site in Beijing during the summer of 2016. High levels of $ClNO_2$ and N_2O_5 were observed, with maxima of 2.9 ppbv and 937 pptv (1-min), respectively. The N_2O_5 uptake coefficient was estimated to be in the range of 0.010-0.055, with an average value of 0.034 ± 0.018, and the corresponding $ClNO_2$ yield was derived

to be in the range of 0.5-1.0, with an average value of 0.73 ± 0.25. The elevated $ClNO_2$ levels and $ClNO_2/N_2O_5$ ratios are comparable with those in chloride-rich regions in the NCP. The results highlight fast N_2O_5 heterogeneous hydrolysis and efficient $ClNO_2$ formation in the outflow of urban Beijing. Thus, its role in O_3 pollution in summer could be more important than in other regions.

Since the NO_3-N_2O_5 chemical equilibrium favors NO_3 in summer with high temperature and high NO_x, the elevated NO_3 dominated the nocturnal degradation of BVOCs and could lead to efficient ONs formation. Because the air masses in Beijing featured high NO_x/BVOCs ratios (>10), our results suggest that the nocturnal NO_3 oxidation of BVOCs was NO_x-dominated. Because of the extremely high NO_x emissions, the formation of ONs may not be sensitive to the reduction of NO_x but rather to the change of unsaturated VOCs (e.g., BVOCs), which is similar to the daytime photochemical O_3 pollution (e.g., Lu et al., 2010) diagnosed for this area; this suggests that the control of the unsaturated VOCs would moderate the O_3 pollution and ONs particulate matter in parallel. Moreover, the reduction of NO_x would also be helpful to reduce the pNO_3^- formation via N_2O_5 heterogeneous hydrolysis under such high NO_x/BVOCs ratios (Edwards et al., 2017).

Acknowledgements. This work was supported by the National Natural Science Foundation of China (Grants No. 91544225, 41375124, 21522701, 41421064, 91744204), the National Science and Technology Support Program of China (No. 2014BAC21B01), the Strategic Priority Research Program of the Chinese Academy of Sciences (Grants No. XDB05010500), and the program on "Photochemical smog in China" financed by the Swedish Research Council (639-2013-6917). The authors gratefully acknowledge the Peking University and Gethenburg University science team for their technical support and discussions during the Changping campaign.

Reference

Allan, B. J., Carslaw, N., Coe, H., Burgess, R. A., and Plane, J. M. C.: Observations of the nitrate radical in the marine boundary layer, J Atmos Chem, 33, 129-154, Doi10.1023/A:1005917203307, 1999.

Bannan, T. J., Booth, A. M., Bacak, A., Muller, J. B. A., Leather, K. E., Le Breton, M., Jones, B., Young, D., Coe, H., Allan, J., Visser, S., Slowik, J. G., Furger, M., Prevot, A. S. H., Lee, J., Dunmore, R. E., Hopkins, J. R., Hamilton, J. F., Lewis, A. C., Whalley, L. K., Sharp, T., Stone, D., Heard, D. E., Fleming, Z. L., Leigh, R., Shallcross, D. E., and Percival, C. J.: The first UK measurements of nitryl chloride using a chemical ionization mass spectrometer in central London in the summer of 2012, and an investigation of the role of Cl atom oxidation, J Geophys Res-Atmos, 120, 5638-5657, 10.1002/2014jd022629, 2015.

Benton, A. K., Langridge, J. M., Ball, S. M., Bloss, W. J., Dall'Osto, M., Nemitz, E., Harrison, R. M., and Jones, R. L.: Night-time chemistry above London: measurements of NO_3 and N_2O_5 from the BT Tower, Atmos Chem Phys, 10, 9781-9795, 10.5194/acp-10-9781-2010, 2010.

Bertram, T. H., and Thornton, J. A.: Toward a general parameterization of N_2O_5 reactivity on aqueous particles: the competing effects of particle liquid water, nitrate and chloride, Atmos Chem Phys, 9, 8351-8363, 2009.

Bertram, T. H., Thornton, J. A., Riedel, T. P., Middlebrook, A. M., Bahreini, R., Bates, T. S., Quinn, P. K., and Coffman, D. J.: Direct observations of N_2O_5 reactivity on ambient aerosol particles, Geophys Res Lett, 36, Artn L19803.10.1029/2009gl040248, 2009.

Bohn, B., Corlett, G. K., Gillmann, M., Sanghavi, S., Stange, G., Tensing, E., Vrekoussis, M., Bloss, W. J., Clapp, L. J., Kortner,M., Dorn, H.-P., Monks, P. S., Platt, U., Plass-Dülmer, C., Mihalopoulos, N., Heard, D. E., Clemitshaw, K. C., Meixner, F. X.,Prevot, A. S. H., and Schmitt, R.: Photolysis frequency measurement techniques: results of a comparison within the ACCENTproject, Atmos. Chem. Phys., 8, 5373–5391, doi:10.5194/acp-8-5373-2008, 2008.

Behnke, W., George, C., Scheer, V., and Zetzsch, C.: Production and decay of ClNO2, from the reaction of gaseous N2O5 with NaCl solution: Bulk and aerosol experiments, J Geophys Res-Atmos, 102, 3795-3804, Doi 10.1029/96jd03057, 1997.

Boyd, C. M., Nah, T., Xu, L., Berkemeier, T., and Ng, N. L.: Secondary Organic Aerosol (SOA) from Nitrate Radical Oxidation of Monoterpenes: Effects of Temperature, Dilution, and Humidity on Aerosol Formation, Mixing, and Evaporation, Environ Sci Technol, 51, 7831-7841, 2017.

Brown, S. S., Stark, H., and Ravishankara, A. R.: Applicability of the steady state approximation to the interpretation of atmospheric observations of NO_3 and N_2O_5, J Geophys Res-Atmos, 108, Artn 4539.Doi 10.1029/2003jd003407, 2003.

Brown, S. S., Ryerson, T. B., Wollny, A. G., Brock, C. A., Peltier, R., Sullivan, A. P., Weber, R. J., Dube, W. P., Trainer, M., Meagher, J. F., Fehsenfeld, F. C., and Ravishankara, A. R.: Variability in nocturnal nitrogen oxide processing and its role in regional air quality, Science, 311, 67-70, DOI 10.1126/science.1120120, 2006.

Brown, S. S., Dube, W. P., Fuchs, H., Ryerson, T. B., Wollny, A. G., Brock, C. A., Bahreini, R., Middlebrook, A. M., Neuman, J. A., Atlas, E., Roberts, J. M., Osthoff, H. D., Trainer, M., Fehsenfeld, F. C., and Ravishankara, A. R.: Reactive uptake coefficients for N_2O_5 determined from aircraft measurements during the Second Texas Air Quality Study: Comparison to current model parameterizations, J Geophys Res-Atmos, 114, Artn D00f10. Doi 10.1029/2008jd011679, 2009.

Brown, S. S., and Stutz, J.: Nighttime radical observations and chemistry, Chem Soc Rev, 41, 6405-6447, Doi 10.1039/C2cs35181a, 2012.

Brown, S. S., Dube, W. P., Tham, Y. J., Zha, Q. Z., Xue, L. K., Poon, S., Wang, Z., Blake, D. R., Tsui, W., Parrish, D. D., and Wang, T.: Nighttime chemistry at a high altitude site above Hong Kong, J Geophys Res-Atmos, 121, 2457-2475, 10.1002/2015jd024566, 2016.

Chang, W. L., Bhave, P. V., Brown, S. S., Riemer, N., Stutz, J., and Dabdub, D.: Heterogeneous Atmospheric Chemistry, Ambient Measurements, and Model Calculations of N_2O_5: A Review, Aerosol Sci Tech, 45, 665-695, 2011.

DeCarlo, P. F., Kimmel, J., Trimborn, A., Northway, M., Jayne, J. T., Aiken, A., Gonin, M., Fuhrer, K., Horvath, T., Docherty, K., Worsnop, D. R., and Jimenez, J. L.: Field-deployable, high-resolution, time-of-flight Aerosol Mass Spectrometer, Anal. Chem., 78, 8281-8289, 2006.

de Gouw, J. and Warneke, C.: Measurements of volatile organic compounds in the earth's atmosphere using proton-transferreaction mass spectrometry, Mass Spectrom. Rev., 26, 223-257, 2007.

Draxler, R. R., and G. D. Rolph: HYSPLIT (HYbrid Single-Particle Lagrangian Integrated Tracker) Model access via NOAA ARL Ready Website [Available at http://www.arl.noaa.gov/ready/hysplit4.html, NOAA Air Resources Laboratory, Silver Spring, MD]. 2003.

Edwards, P. M., Aikin, K. C., Dube, W. P., Fry, J. L., Gilman, J. B., de Gouw, J. A., Graus, M. G., Hanisco, T. F., Holloway, J., Huber, G., Kaiser, J., Keutsch, F. N., Lerner, B. M., Neuman, J. A., Parrish, D. D., Peischl, J., Pollack, I. B., Ravishankara, A. R., Roberts, J. M., Ryerson, T. B., Trainer, M., Veres, P. R., Wolfe, G. M., Warneke, C., and Brown, S. S.: Transition from high- to low-NOx control of night-time oxidation in the southeastern US, Nat Geosci, 10, 490-+, 10.1038/Ngeo2976, 2017.

Faxon, C. B., Bean, J. K., and Ruiz, L. H.: Inland Concentrations of Cl_2 and $ClNO_2$ in Southeast Texas suggest chlorine chemistry significantly contributes to atmospheric reactivity, Atmosphere, 6, 1487–1506, 2015.

Finlayson-Pitts, B. J., Ezell, M. J., and Pitts, J. N.: Formation of Chemically Active Chlorine Compounds by Reactions of Atmospheric Nacl Particles with Gaseous N_2O_5 and $ClONO_2$, Nature, 337, 241-244, DOI 10.1038/337241a0, 1989.

Fry, J. L., Kiendler-Scharr, A., Rollins, A. W., Wooldridge, P. J., Brown, S. S., Fuchs, H., Dube, W., Mensah, A., dal Maso, M., Tillmann, R., Dorn, H. P., Brauers, T., and Cohen, R. C.: Organic nitrate and secondary organic aerosol yield from NO_3 oxidation of beta-pinene evaluated using a gas-phase kinetics/aerosol partitioning model, Atmos Chem Phys, 9, 1431-1449, 2009.

Gaston, C. J., Thornton, J. A., and Ng, N. L.: Reactive uptake of N_2O_5 to internally mixed inorganic and organic particles: the role of organic carbon oxidation state and inferred organic phase separations, Atmos Chem Phys, 14, 5693-5707, 10.5194/acp-14-5693-2014, 2014.

Geyer, A., Alicke, B., Konrad, S., Schmitz, T., Stutz, J., and Platt, U.: Chemistry and oxidation capacity of the nitrate radical in the continental boundary layer near Berlin, J Geophys Res-Atmos, 106, 8013-8025, Doi 10.1029/2000jd900681, 2001.

Goliff, W. S., Stockwell, W. R., and Lawson, C. V.: The regional atmospheric chemistry mechanism, version 2, Atmos Environ, 68, 174-185, 2013.

Grzinic, G., Bartels-Rausch, T., Berkemeier, T., Turler, A., and Ammann, M.: Viscosity controls humidity dependence of N_2O_5 uptake to citric acid aerosol, Atmos Chem Phys, 15, 13615-13625, 2015.

Hallquist, M., Stewart, D. J., Stephenson, S. K., and Cox, R. A.: Hydrolysis of N_2O_5 on sub-micron sulfate aerosols, Phys Chem Chem Phys, 5, 3453-3463, Doi 10.1039/B301827j, 2003.

Hallquist, M., Munthe, J., Hu, M., Wang, T., Chan, C. K., Gao, J., Boman, J., Guo, S., Hallquist, A. M., Mellqvist, J., Moldanova, J., Pathak, R. K., Pettersson, J. B. C., Pleijel, H., Simpson, D., and Thynell, M.: Photochemical smog in China: scientific challenges and implications for air-quality policies, Natl Sci Rev, 3, 401-403, 10.1093/nsr/nww080, 2016.

Kiendler-Scharr, A., Mensah, A. A., Friese, E., Topping, D., Nemitz, E., Prevot, A. S. H., Aijala, M., Allan, J., Canonaco, F., Canagaratna, M., Carbone, S., Crippa, M., Dall Osto, M., Day, D. A., De Carlo, P., Di Marco, C.

F., Elbern, H., Eriksson, A., Freney, E., Hao, L., Herrmann, H., Hildebrandt, L., Hillamo, R., Jimenez, J. L., Laaksonen, A., McFiggans, G., Mohr, C., O'Dowd, C., Otjes, R., Ovadnevaite, J., Pandis, S. N., Poulain, L., Schlag, P., Sellegri, K., Swietlicki, E., Tiitta, P., Vermeulen, A., Wahner, A., Worsnop, D., and Wu, H. C.: Ubiquity of organic nitrates from nighttime chemistry in the European submicron aerosol, Geophys Res Lett, 43, 7735-7744, 2016.

Le Breton, M., Bacak, A., Muller, J. B. A., Bannan, T. J., Kennedy, O., Ouyang, B., Xiao, P., Bauguitte, S. J. B., Shallcross, D. E., Jones, R. L., Daniels, M. J. S., Ball, S. M., and Percival, C. J.: The first airborne comparison of N_2O_5 measurements over the UK using a CIMS and BBCEAS during the RONOCO campaign, Anal Methods-Uk, 6, 9731-9743, 10.1039/c4ay02273d, 2014.

Le Breton, M., Hallquist, Å. M., Pathak, R. K., Simpson, D., Wang, Y., Johansson, J., Zheng, J., Yang, Y., Shang, D., Wang, H., Liu, Q., Chan, C., Wang, T., Bannan, T. J., Priestley, M., Percival, C. J., Shallcross, D. E., Lu, K., Guo, S., Hu, M., and Hallquist, M.: Chlorine oxidation of VOCs at a semi-rural site in Beijing: Significant chlorine liberation from $ClNO_2$ and subsequent gas and particle phase Cl-VOC production, Atmos. Chem. Phys. Discuss., 2018, 1-25, 2018.

Li, S. W., Liu, W. Q., Xie, P. H., Qin, M., and Yang, Y. J.: Observation of Nitrate Radical in the Nocturnal Boundary Layer During a Summer Field Campaign in Pearl River Delta, China, Terr Atmos Ocean Sci, 23, 39-48, Doi 10.3319/Tao.2011.07.26.01(a), 2012.

Li, Q. Y., Zhang, L., Wang, T., Tham, Y. J., Ahmadov, R., Xue, L. K., Zhang, Q., and Zheng, J. Y.: Impacts of heterogeneous uptake of dinitrogen pentoxide and chlorine activation on ozone and reactive nitrogen partitioning: improvement and application of the WRF-Chem model in southern China, Atmos Chem Phys, 16, 14875-14890, 10.5194/acp-16-14875-2016, 2016.

Liu, X. G., Gu, J. W., Li, Y. P., Cheng, Y. F., Qu, Y., Han, T. T., Wang, J. L., Tian, H. Z., Chen, J., and Zhang, Y. H.: Increase of aerosol scattering by hygroscopic growth: Observation, modeling, and implications on visibility, Atmos Res, 132, 91-101, 10.1016/j.atmosres.2013.04.007, 2013.

Liu, M. X., Song, Y., Zhou, T., Xu, Z. Y., Yan, C. Q., Zheng, M., Wu, Z. J., Hu, M., Wu, Y. S., and Zhu, T.: Fine particle pH during severe haze episodes in northern China, Geophys Res Lett, 44, 5213-5221, 10.1002/2017gl073210, 2017.

Lopez-Hilfiker, F. D., Mohr, C., Ehn, M., Rubach, F., Kleist, E., Wildt, J., Mentel, T. F., Lutz, A., Hallquist, M., Worsnop, D., and Thornton, J. A.: A novel method for online analysis of gas and particle composition: description and evaluation of a Filter Inlet for Gases and AEROsols (FIGAERO), Atmos Meas Tech, 7, 983-1001, 10.5194/amt-7-983-2014, 2014.

Lu, K. D., Zhang, Y. H., Su, H., Brauers, T., Chou, C. C., Hofzumahaus, A., Liu, S. C., Kita, K., Kondo, Y., Shao, M., Wahner, A., Wang, J. L., Wang, X. S., and Zhu, T.: Oxidant (O_3 + NO_2) production processes and formation regimes in Beijing, J Geophys Res-Atmos, 115, 2010.

McLaren, R., Wojtal, P., Majonis, D., McCourt, J., Halla, J. D., and Brook, J.: NO_3 radical measurements in a polluted marine environment: links to ozone formation, Atmos Chem Phys, 10, 4187-4206, 10.5194/acp-10-4187-2010, 2010.

Mentel, T. F., Sohn, M., and Wahner, A.: Nitrate effect in the heterogeneous hydrolysis of dinitrogen pentoxide on aqueous aerosols, Phys Chem Chem Phys, 1, 5451-5457, Doi 10.1039/A905338g, 1999.

Mielke, L. H., Furgeson, A., and Osthoff, H. D.: Observation of $ClNO_2$ in a Mid-Continental Urban Environment, Environ Sci Technol, 45, 8889-8896, 10.1021/es201955u, 2011.

Mielke, L. H., Stutz, J., Tsai, C., Hurlock, S. C., Roberts, J. M., Veres, P. R., Froyd, K. D., Hayes, P. L., Cubison, M. J., Jimenez, J. L., Washenfelder, R. A., Young, C. J., Gilman, J. B., de Gouw, J. A., Flynn, J. H., Grossberg, N., Lefer, B. L., Liu, J., Weber, R. J., and Osthoff, H. D.: Heterogeneous formation of nitryl chloride and its role as a nocturnal NOx reservoir species during CalNex-LA 2010, J Geophys Res-Atmos, 118, 10638-10652, Doi 10.1002/Jgrd.50783, 2013.

Morgan, W. T., Ouyang, B., Allan, J. D., Aruffo, E., Di Carlo, P., Kennedy, O. J., Lowe, D., Flynn, M. J., Rosenberg, P. D., Williams, P. I., Jones, R., McFiggans, G. B., and Coe, H.: Influence of aerosol chemical composition on N_2O_5 uptake: airborne regional measurements in northwestern Europe, Atmos Chem Phys, 15, 973-990, DOI 10.5194/acp-15-973-2015, 2015.

Ng, N. L., Kwan, A. J., Surratt, J. D., Chan, A. W. H., Chhabra, P. S., Sorooshian, A., Pye, H. O. T., Crounse, J. D., Wennberg, P. O., Flagan, R. C., and Seinfeld, J. H.: Secondary organic aerosol (SOA) formation from reaction of isoprene with nitrate radicals (NO3), Atmos Chem Phys, 8, 4117-4140, 2008.

Ng, N. L., Brown, S. S., Archibald, A. T., Atlas, E., Cohen, R. C., Crowley, J. N., Day, D. A., Donahue, N. M., Fry, J. L., Fuchs, H., Griffin, R. J., Guzman, M. I., Herrmann, H., Hodzic, A., Iinuma, Y., Jimenez, J. L., Kiendler-Scharr, A., Lee, B. H., Luecken, D. J., Mao, J. Q., McLaren, R., Mutzel, A., Osthoff, H. D., Ouyang, B., Picquet-Varrault, B., Platt, U., Pye, H. O. T., Rudich, Y., Schwantes, R. H., Shiraiwa, M., Stutz, J., Thornton, J. A., Tilgner, A., Williams, B. J., and Zaveri, R. A.: Nitrate radicals and biogenic volatile organic compounds: oxidation, mechanisms, and organic aerosol, Atmos Chem Phys, 17, 2103-2162, 10.5194/acp-17-2103-2017, 2017.

Osthoff, H. D., Roberts, J. M., Ravishankara, A. R., Williams, E. J., Lerner, B. M., Sommariva, R., Bates, T. S., Coffman, D., Quinn, P. K., Dibb, J. E., Stark, H., Burkholder, J. B., Talukdar, R. K., Meagher, J., Fehsenfeld, F. C., and Brown, S. S.: High levels of nitryl chloride in the polluted subtropical marine boundary layer, Nat Geosci, 1, 324-328, Doi 10.1038/Ngeo177, 2008.

Phillips, G. J., Thieser, J., Tang, M. J., Sobanski, N., Schuster, G., Fachinger, J., Drewnick, F., Borrmann, S., Bingemer, H., Lelieveld, J., and Crowley, J. N.: Estimating N_2O_5 uptake coefficients using ambient measurements of NO_3, N_2O_5, $ClNO_2$ and particle-phase nitrate, Atmos Chem Phys, 16, 13231-13249, 10.5194/acp-16-13231-2016, 2016.

Platt, U., Perner, D., Winer, A. M., Harris, G. W., and Pitts, J. N.: Detection of NO_3 in the Polluted Troposphere by Differential Optical-Absorption, Geophys Res Lett, 7, 89-92, Doi 10.1029/Gl007i001p00089, 1980.

Pye, H. O. T., Chan, A. W. H., Barkley, M. P., and Seinfeld, J. H.: Global modeling of organic aerosol: the importance of reactive nitrogen (NOx and NO_3), Atmos Chem Phys, 10, 11261-11276, 2010.

Riedel, T. P., Bertram, T. H., Ryder, O. S., Liu, S., Day, D. A., Russell, L. M., Gaston, C. J., Prather, K. A., and Thornton, J. A.: Direct N2O5 reactivity measurements at a polluted coastal site, Atmos Chem Phys, 12, 2959-2968, DOI 10.5194/acp-12-2959-2012, 2012.

Riedel, T. P., Wolfe, G. M., Danas, K. T., Gilman, J. B., Kuster, W. C., Bon, D. M., Vlasenko, A., Li, S. M., Williams, E. J., Lerner, B. M., Veres, P. R., Roberts, J. M., Holloway, J. S., Lefer, B., Brown, S. S., and Thornton, J. A.: An MCM modeling study of nitryl chloride ($ClNO_2$) impacts on oxidation, ozone production and nitrogen oxide partitioning in polluted continental outflow, Atmos Chem Phys, 14, 3789-3800, 10.5194/acp-14-3789-2014, 2014.

Riemer, N., Vogel, H., Vogel, B., Anttila, T., Kiendler-Scharr, A., and Mentel, T. F.: Relative importance of organic coatings for the heterogeneous hydrolysis of N2O5 during summer in Europe, J Geophys Res-Atmos, 114, 2009.

Roberts, J. M., Osthoff, H. D., Brown, S. S., Ravishankara, A. R., Coffman, D., Quinn, P., and Bates, T.: Laboratory studies of products of N_2O_5 uptake on Cl^- containing substrates, Geophys Res Lett, 36, Artn L20808. 10.1029/2009gl040448, 2009.

Rollins, A. W., Kiendler-Scharr, A., Fry, J. L., Brauers, T., Brown, S. S., Dorn, H. P., Dube, W. P., Fuchs, H., Mensah, A., Mentel, T. F., Rohrer, F., Tillmann, R., Wegener, R., Wooldridge, P. J., and Cohen, R. C.: Isoprene oxidation by nitrate radical: alkyl nitrate and secondary organic aerosol yields, Atmos Chem Phys, 9, 6685-6703, 2009.

Sarwar, G., Simon, H., Xing, J., and Mathur, R.: Importance of tropospheric $ClNO_2$ chemistry across the Northern Hemisphere, Geophys Res Lett, 41, 4050-4058, 10.1002/2014gl059962, 2014.

Spittler, M., Barnes, I., Bejan, I., Brockmann, K. J., Benter, T., and Wirtz, K.: Reactions of NO_3 radicals with limonene and alpha-pinene: Product and SOA formation, Atmos Environ, 40, S116-S127, 10.1016/j.atmosenv.2005.09.093, 2006.

Stutz, J., Wong, K. W., Lawrence, L., Ziemba, L., Flynn, J. H., Rappengluck, B., and Lefer, B.: Nocturnal NO_3 radical chemistry in Houston, TX, Atmos Environ, 44, 4099-4106, 10.1016/j.atmosenv.2009.03.004, 2010.

Su, X., Tie, X. X., Li, G. H., Cao, J. J., Huang, R. J., Feng, T., Long, X., and Xu, R. G.: Effect of hydrolysis of N_2O_5 on nitrate and ammonium formation in Beijing China: WRF-Chem model simulation, Sci Total Environ, 579, 221-229, 10.1016/j.scitotenv.2016.11.125, 2017.

Tan, Z., Fuchs, H., Lu, K., Hofzumahaus, A., Bohn, B., Broch, S., Dong, H., Gomm, S., Häseler, R., He, L., Holland, F., Li, X., Liu, Y., Lu, S., Rohrer, F., Shao, M., Wang, B., Wang, M., Wu, Y., Zeng, L., Zhang, Y., Wahner, A., and Zhang, Y.: Radical chemistry at a rural site (Wangdu) in the North China Plain: observation and model calculations of OH, HO_2 and RO_2 radicals, Atmos. Chem. Phys., 17, 663-690, 10.5194/acp-17-663-2017, 2017.

Tang, M. J., Schuster, G., and Crowley, J. N.: Heterogeneous reaction of N_2O_5 with illite and Arizona test dust particles, Atmos Chem Phys, 14, 245-254, 2014.

Tang, M. J., Thieser, J., Schuster, G., and Crowley, J. N.: Kinetics and mechanism of the heterogeneous reaction of N_2O_5 with mineral dust particles, Phys Chem Chem Phys, 14, 8551-8561, 2012.

Tham, Y. J., Wang, Z., Li, Q. Y., Yun, H., Wang, W. H., Wang, X. F., Xue, L. K., Lu, K. D., Ma, N., Bohn, B., Li, X., Kecorius, S., Gross, J., Shao, M., Wiedensohler, A., Zhang, Y. H., and Wang, T.: Significant concentrations of

nitryl chloride sustained in the morning: investigations of the causes and impacts on ozone production in a polluted region of northern China, Atmos Chem Phys, 16, 14959-14977, 10.5194/acp-16-14959-2016, 2016.

Thornton, J. A., Braban, C. F., and Abbatt, J. P. D.: N_2O_5 hydrolysis on sub-micron organic aerosols: the effect of relative humidity, particle phase, and particle size, Phys Chem Chem Phys, 5, 4593-4603, Doi 10.1039/B307498f, 2003.

Thornton, J. A., and Abbatt, J. P. D.: N_2O_5 reaction on submicron sea salt aerosol: Kinetics, products, and the effect of surface active organics, J Phys Chem A, 109, 10004-10012, Doi 10.1021/Jp054183t, 2005.

Thornton, J. A., Kercher, J. P., Riedel, T. P., Wagner, N. L., Cozic, J., Holloway, J. S., Dube, W. P., Wolfe, G. M., Quinn, P. K., Middlebrook, A. M., Alexander, B., and Brown, S. S.: A large atomic chlorine source inferred from mid-continental reactive nitrogen chemistry, Nature, 464, 271-274, Doi 10.1038/Nature08905, 2010.

Wagner, N. L., Riedel, T. P., Young, C. J., Bahreini, R., Brock, C. A., Dube, W. P., Kim, S., Middlebrook, A. M., Ozturk, F., Roberts, J. M., Russo, R., Sive, B., Swarthout, R., Thornton, J. A., VandenBoer, T. C., Zhou, Y., and Brown, S. S.: N_2O_5 uptake coefficients and nocturnal NO_2 removal rates determined from ambient wintertime measurements, J Geophys Res-Atmos, 118, 9331-9350, Doi 10.1002/Jgrd.50653, 2013.

Wahner, A., Mentel, T. F., and Sohn, M.: Gas-phase reaction of N_2O_5 with water vapor: Importance of heterogeneous hydrolysis of N_2O_5 and surface desorption of HNO3 in a large teflon chamber, Geophys Res Lett, 25, 2169-2172, Doi 10.1029/98gl51596, 1998.

Wang, S. S., Shi, C. Z., Zhou, B., Zhao, H., Wang, Z. R., Yang, S. N., and Chen, L. M.: Observation of NO_3 radicals over Shanghai, China, Atmos Environ, 70, 401-409, DOI 10.1016/j.atmosenv.2013.01.022, 2013.

Wang, M., Shao, M., Chen, W., Yuan, B., Lu, S., Zhang, Q., Zeng, L., and Wang, Q.: A temporally and spatially resolved validation of emission inventories by measurements of ambient volatile organic compounds in Beijing, China, Atmos Chem Phys, 14, 5871-5891, 10.5194/acp-14-5871-2014, 2014.

Wang, D., Hu, R. Z., Xie, P. H., Liu, J. G., Liu, W. Q., Qin, M., Ling, L. Y., Zeng, Y., Chen, H., Xing, X. B., Zhu, G. L., Wu, J., Duan, J., Lu, X., and Shen, L. L.: Diode laser cavity ring-down spectroscopy for in situ measurement of NO3 radical in ambient air, J Quant Spectrosc Ra, 166, 23-29, 10.1016/j.jqsrt.2015.07.005, 2015.

Wang, H. C., and Lu, K. D.: Determination and Parameterization of the Heterogeneous Uptake Coefficient of Dinitrogen Pentoxide (N_2O_5), Prog Chem, 28, 917-933, 10.7536/Pc151225, 2016.

Wang, T., Tham, Y. J., Xue, L. K., Li, Q. Y., Zha, Q. Z., Wang, Z., Poon, S. C. N., Dube, W. P., Blake, D. R., Louie, P. K. K., Luk, C. W. Y., Tsui, W., and Brown, S. S.: Observations of nitryl chloride and modeling its source and effect on ozone in the planetary boundary layer of southern China, J Geophys Res-Atmos, 121, 2476-2489, 10.1002/2015jd024556, 2016.

Wang, H. C., Chen, J., and Lu, K. D.: Development of a portable cavity-enhanced absorption spectrometer for the measurement of ambient NO_3 and N_2O_5: experimental setup, lab characterizations, and field applications in a polluted urban environment, Atmos Meas Tech, 10, 1465-1479, 10.5194/amt-10-1465-2017, 2017a.

Wang, H. C., Lu, K. D., Tan, Z. F., Sun, K., Li, X., Hu, M., Shao, M., Zeng, L. M., Zhu, T., and Zhang, Y. H.: Model simulation of NO_3, N_2O_5 and $ClNO_2$ at a rural site in Beijing during CAREBeijing-2006, Atmos Res, 196, 97-107, 10.1016/j.atmosres.2017.06.013, 2017b.

Wang, H. C., Lu, K. D., Chen, X. R., Zhu, Q. D., Chen, Q., Guo, S., Jiang, M. Q., Li, X., Shang, D. J., Tan, Z. F: High N2O5 concentrations observed in urban Beijing: Implications of a large nitrate formation pathway., Environ. Sci. Technol. Lett., 10, doi: 10.1021/acs.estlett.7b00341, 2017c.

Wang, X. F., Wang, H., Xue, L. K., Wang, T., Wang, L. W., Gu, R. R., Wang, W. H., Tham, Y. J., Wang, Z., Yang, L. X., Chen, J. M., and Wang, W. X.: Observations of N_2O_5 and $ClNO_2$ at a polluted urban surface site in North China: High N_2O_5 uptake coefficients and low $ClNO_2$ product yields, Atmos Environ, 156, 125-134, 10.1016/j.atmosenv.2017.02.035, 2017.

Wang, Z., Wang, W. H., Tham, Y. J., Li, Q. Y., Wang, H., Wen, L., Wang, X. F., and Wang, T.: Fast heterogeneous N_2O_5 uptake and $ClNO_2$ production in power plant and industrial plumes observed in the nocturnal residual layer over the North China Plain, Atmos Chem Phys, 17, 12361-12378, 2017. 10.5194/acp-17-12361-2017

Wayne, R. P., Barnes, I., Biggs, P., Burrows, J. P., Canosamas, C. E., Hjorth, J., Lebras, G., Moortgat, G. K., Perner, D., Poulet, G., Restelli, G., and Sidebottom, H.: The Nitrate Radical - Physics, Chemistry, and the Atmosphere, Atmos Environ a-Gen, 25, 1-203, Doi 10.1016/0960-1686(91)90192-A, 1991.

Xue, L. K., Saunders, S. M., Wang, T., Gao, R., Wang, X. F., Zhang, Q. Z., and Wang, W. X.: Development of a chlorine chemistry module for the Master Chemical Mechanism, Geosci Model Dev, 8, 3151-3162, 10.5194/gmd-8-3151-2015, 2015.

Ye, N. N. L., K. D. Dong, H. B. Wu, Y. S. Zeng, L. M and Zhang, Y. H.: A study of the Water-Soluble Inorgic Salts and Their Gases Precursors at Wangdu Site in the Summer Time, Acta Scientiarum Naturalium Universitatis, 52, p1109-1117, doi.org/10.13209/j.0479-8023.2016.116, 2016.

Yue, D. L., Hu, M., Wu, Z. J., Wang, Z. B., Guo, S., Wehner, B., Nowak, A., Achtert, P., Wiedensohler, A., Jung, J., Kim, Y. J., and Liu, S.: Characteristics of aerosol size distributions and new particle formation in the summer in Beijing, J Geophys Res-Atmos, 114, Artn D00g1210.1029/2008jd010894, 2009.

Zheng, J., Hu, M., Du, Z. F., Shang, D. J., Gong, Z. H., Qin, Y. H., Fang, J. Y., Gu, F. T., Li, M. R., Peng, J. F., Li, J., Zhang, Y. Q., Huang, X. F., He, L. Y., Wu, Y. S., and Guo, S.: Influence of biomass burning from South Asia at a high-altitude mountain receptor site in China, Atmos Chem Phys, 17, 6853-6864, 10.5194/acp-17-6853-2017, 2017.

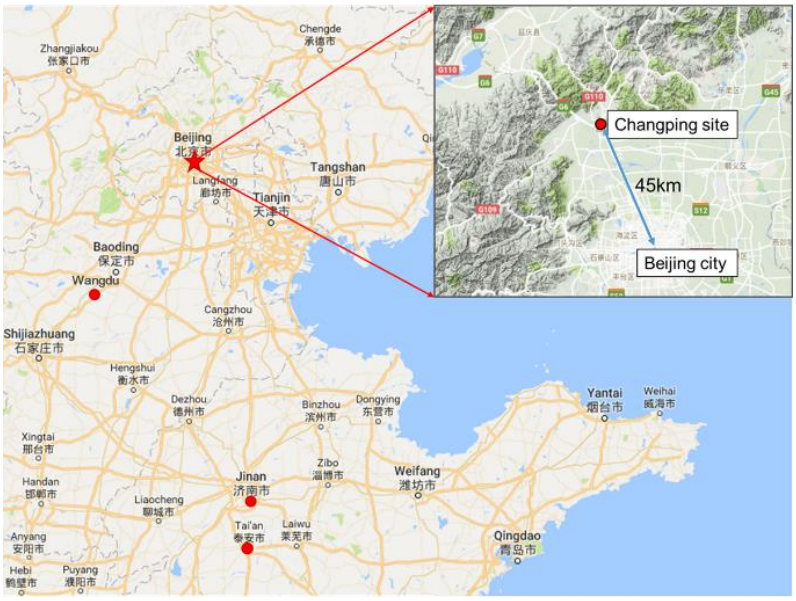

786

787 **Figure 1.** Map of Beijing and surrounding area. The red star shows the location of the Changping site,
788 and red dots show other sites where previous N_2O_5 measurements were conducted in the North China
789 Plain (NCP), including Wangdu, Jinan and Mt. Tai (Tai' an).

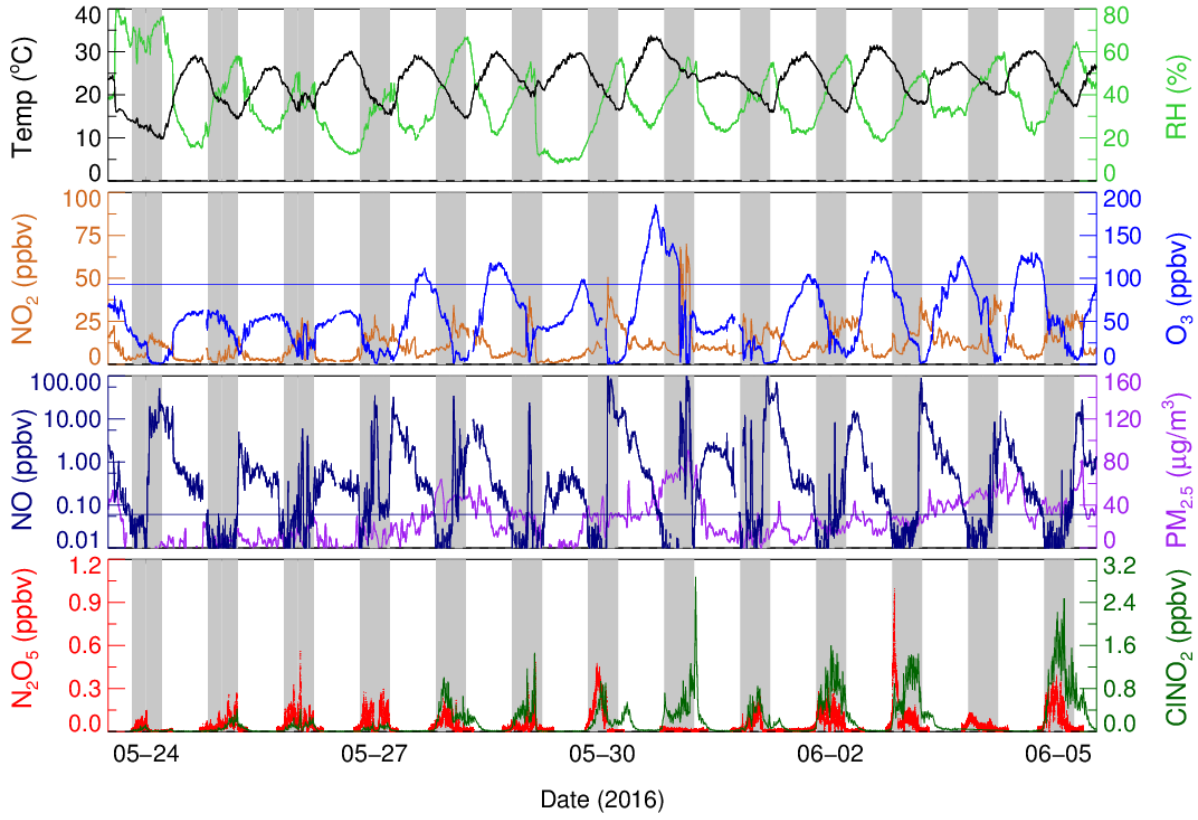

790

791 **Figure 2.** Time series of N_2O_5, $ClNO_2$ and other relevant parameters. The blue line in the O_3 panel
792 denotes Chinese national air quality standard for O_3 (ca. 93 ppbv for the surface conditions). The
793 black line in the NO panel denotes 0.06 ppbv.

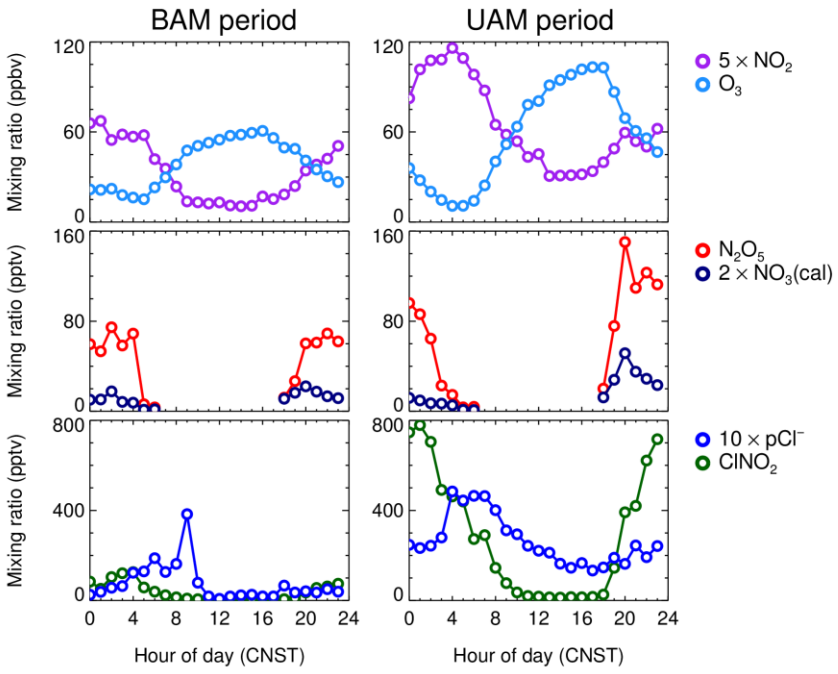

794

795 **Figure 3.** Mean diurnal profiles of 5×NO_2, O_3, N_2O_5, 2×NO_3 (calculated), $ClNO_2$, and 10×pCl^-. The
796 left three panels depict the background air mass (BAM) period and the right three panels depict the
797 urban air mass (UAM) period.

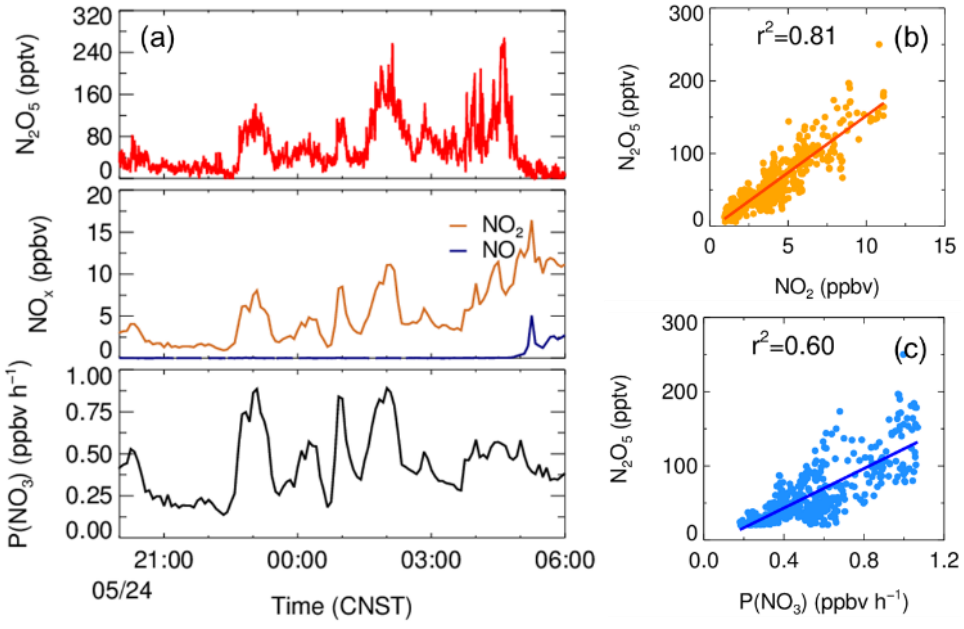

798

799 **Figure 4.** The correlation of the mixing ratio of N_2O_5 and NO_2 and the production rate of NO_3 on the
800 night of May 24.
801

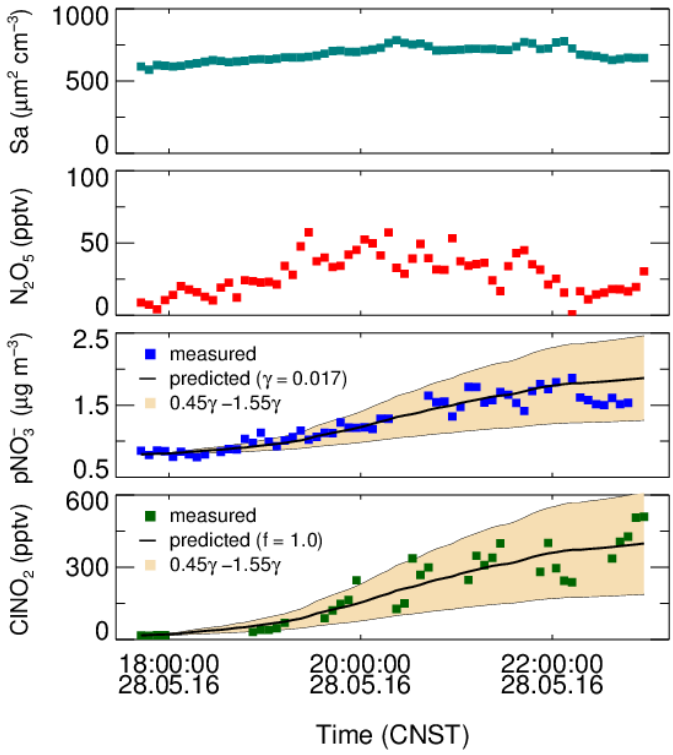

802

803 **Figure 5**. The best fit of γ and f to reproduce the observed $ClNO_2$ and pNO_3^- with an offset on May 28.
804 The black lines are the predicted results of the integrated NO_3^- and $ClNO_2$ by using the observed S_a
805 and N_2O_5.

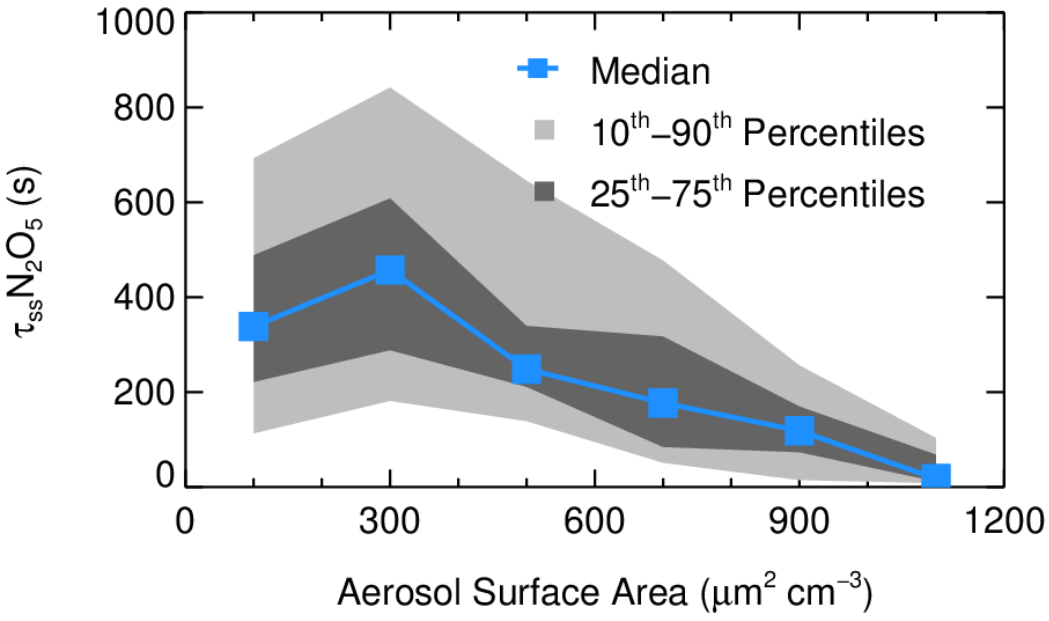

806

807 **Figure 6.** The dependence of N_2O_5 lifetime on aerosol surface area. Data were selected from 20:00 to
808 04:00 and are shown as medians, 25 - 75th percentile ranges, and 10 - 90th percentile ranges, as shown
809 in the legend.

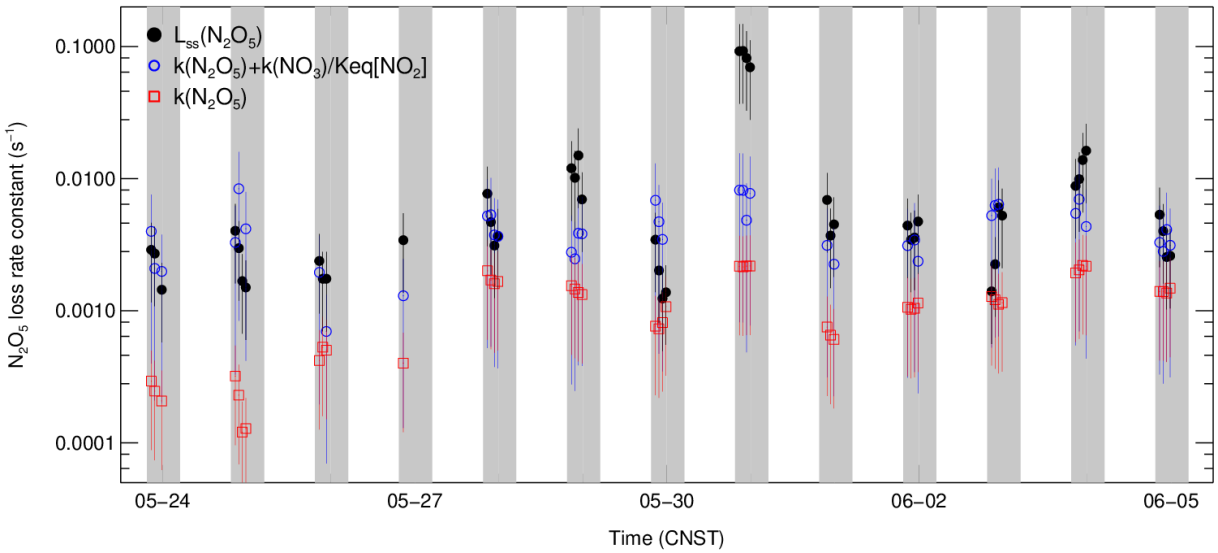

Figure 7. Time series of the individual N_2O_5 loss terms and the loss rate constant of N_2O_5 in steady state (*Lss*(N_2O_5)).

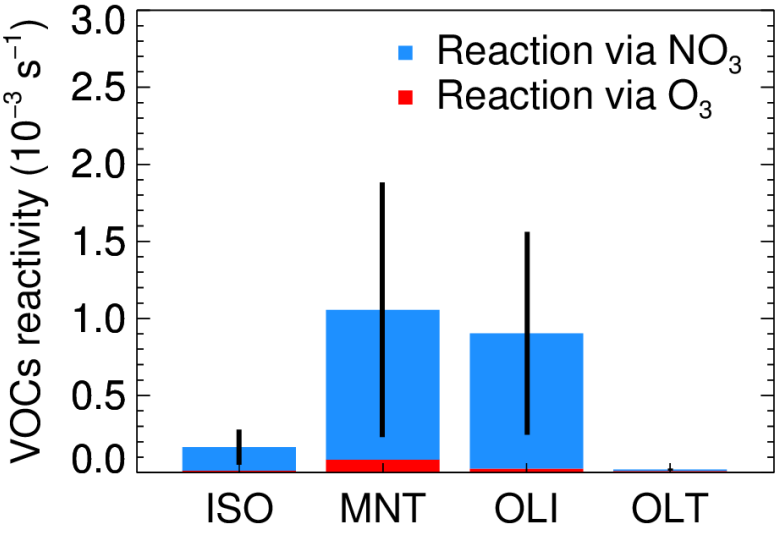

Figure 8. The nighttime VOCs reactivity of NO_3 and O_3 (defined as the pseudo first order loss rate of VOCs initialed by oxidants, include NO_3 and O_3); the VOCs are classified as isoprene (ISO), monoterpene (MNT), the terminal alkenes (OLT) and the internal alkenes (OLI). The data were selected from 20:00 to the next day 04:00.

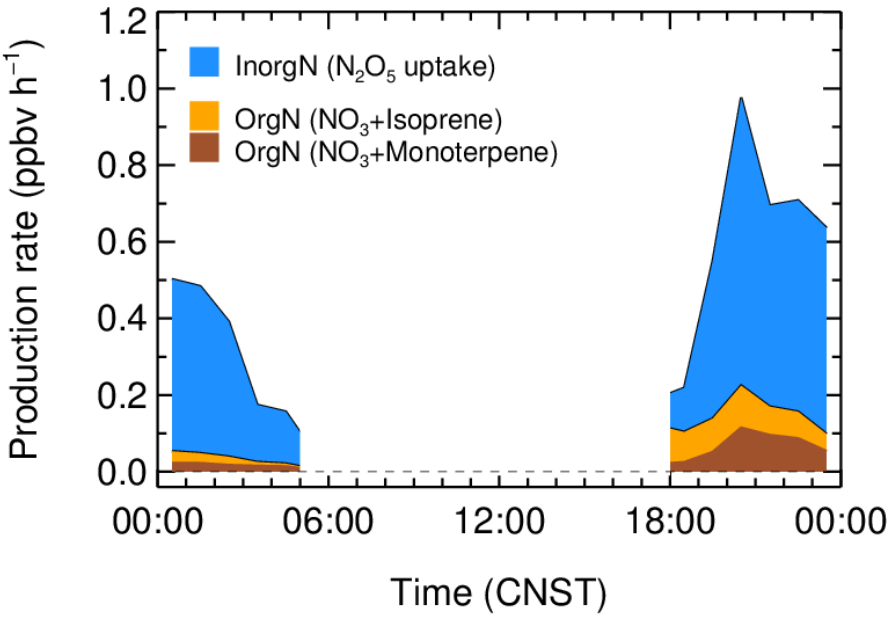

819

820 **Figure 9.** The nighttime production rate of organic and inorganic nitrates; the inorganic nitrates were
821 calculated from the N_2O_5 heterogeneous hydrolysis, and the ONs were calculated by the NO_3 reacted
822 with isoprene and monoterpene.

823

824

825 **Table 1.** The observed gas and particle parameters used in this analysis during the campaign.

Species	Limit of detection	Methods	Accuracy
N_2O_5	2.7 pptv (1σ, 1 min)	CEAS	± 19%
$ClNO_2$	16 pptv (2σ, 1 min)	FIGAERO-ToF-CIMS	± 23%
NO	60 pptv (2σ, 1 min)	Chemiluminescence	± 20%
NO_2	0.3 ppbv (2σ, 1 min)	Mo convert	± 50%
O_3	0.5 ppbv (2σ, 1 min)	UV photometry	± 5%
Aerosol surface area	- (4 min)	SMPS, APS	± 30%
VOCs	0.1 ppbv (5 min)	PTR-MS	± 30%
$PM_{2.5}$	0.1 μg m^{-3} (1 min)	TEOM	± 5%
$PM_{1.0}$ components	0.15 μg m^{-3} (4 min)	HR-ToF-AMS	± 30%

826

827 **Table 2.** Summary of the field observed ambient $ClNO_2/N_2O_5$.

Location	Region	$ClNO_2/N_2O_5$ [a]	References
Beijing, China	Inland	0.7 – 42.0 (5.4)	This work
Wangdu, China	Inland	0.4 - 131.3 (29.5)	Tham et al., 2016
Jinan, China	Marine	25.0 - 118.0 [b]	X. F. Wang et al., 2017
Mt. Tai, China	Marine	~ 4.0	Z. Wang et al., 2017
Hong Kong, China	Marine	0.1 - 2.0	T. Wang et al., 2016
London, UK	Inland	0.02 - 2.4 (0.51)	Bannan et al., 2015
Frankfurt, Germany	Inland	0.2 - 3.0	Phillips et al., 2012
Colorado, USA	Inland	0.2 - 3.0	Thornton et al., 2010
California, USA	Marine	~ 0.2 - 10.0 [c]	Mielke et al., 2013

828 Note: [a] Daily average results; [b] Power plant plume cases at Mt. Tai in Shandong, China; [c] Estimated according to Mielke
829 et al., (2013).

830 **Table 3.** Summary of the average $\gamma \times f$ values derived in the field observations.

Location	Region	$\gamma \times f$	References
Beijing, China	suburban	0.019 ± 0.009	This work
Frankfurt, Germany	suburban	0.014	Phillips et al., 2016
Mt. Tai, China	suburban	0.016	Z. Wang et al., 2017
Jinan, China	urban	<0.008	X. F. Wang et al., 2017
California, USA	urban	0.008	Mielke et al., 2013

831

832 **Table 4.** List of the N_2O_5 uptake coefficients and the yield of $ClNO_2$ in this campaign.

Start time	End time	γ	f
05/25 00:00	05/25 05:00	0.047 ± 0.023	0.60 ± 0.30
05/25 18:30	05/25 23:00	0.012 ± 0.006	1.0 ± 0.50
05/27 19:00	05/27 20:40	0.040 ± 0.032	0.50 ± 0.40
05/28 19:00	05/28 23:00	0.017 ± 0.009	1.0 ± 0.50
05/30 21:00	05/31 00:00	0.055 ± 0.030	0.55 ± 0.30

833